

YbiV From *Escherichia coli* K12 is a HAD Phosphatase

Anne Roberts,^{1,2} Seok-Yong Lee,^{2,3} Emma McCullagh,⁴ Ruth E. Silversmith,⁵ and David E. Wemmer^{1,2*}

¹Department of Chemistry, University of California, Berkeley, California

²Physical Biosciences Division, Lawrence Berkeley National Laboratory, Berkeley, California

³Graduate Group in Biophysics, University of California, Berkeley, California

⁴Department of Molecular and Cellular Biology, University of California, Berkeley, California

⁵Department of Microbiology and Immunology, University of North Carolina at Chapel Hill, Chapel Hill, North Carolina

ABSTRACT The protein YbiV from *Escherichia coli* K12 MG1655 is a hypothetical protein with sequence homology to the haloacid dehalogenase (HAD) superfamily of proteins. Although numerous members of this family have been identified, the functions of few are known. Using the crystal structure, sequence analysis, and biochemical assays, we have characterized YbiV as a HAD phosphatase. The crystal structure of YbiV reveals a two-domain protein, one with the characteristic HAD hydrolase fold, the other an inserted α/β fold. In an effort to understand the mechanism, we also solved and report the structures of YbiV in complex with beryll fluoride (BeF_3^-) and aluminum trifluoride (AlF_3), which have been shown to mimic the phosphorylated intermediate and transition state for hydrolysis, respectively, in analogy to other HAD phosphatases. Analysis of the structures reveals the substrate-binding cavity, which is hydrophilic in nature. Both structure and sequence homology indicate YbiV may be a sugar phosphatase, which is supported by biochemical assays that measured the release of free phosphate on a number of sugar-like substrates. We also investigated available genomic and functional data in an effort to determine the physiological substrate. *Proteins* 2005;58:790–801.

© 2005 Wiley-Liss, Inc.

Key words: phosphatase; YbiV; phosphoaspartate intermediate; HAD superfamily

INTRODUCTION

Members of the haloacid dehalogenase (HAD) superfamily of enzymes comprise a large and diverse set of hydrolases found in the genomes of bacteria, archaea, and eukarya. This family includes phosphatases, phosphonates, P-type ATPases, β -phosphoglucomutases, phosphomannomutases, and dehalogenases, which are involved in cellular processes ranging from amino acid biosynthesis to detoxification.^{1,2} Although sequence identity across the entire HAD family is less than 15%, members share three conserved sequence motifs and a common catalytic mechanism, involving the formation of a covalent intermediate.^{2,3}

Several members of the phosphatase/phosphohydrolase class of HAD proteins have been identified. In these proteins, a conserved aspartic acid residue serves as the

nucleophile in the phosphotransfer reaction, resulting in the formation of a phospho-aspartate intermediate.³ HAD phosphatases are identified by three unique motifs that are conserved in sequence and spatial proximity in the structures. In motif I, **DXDX(T/V)**, the first aspartate forms the phospho-protein intermediate, and also is involved in Mg^{2+} binding (from the sidechain of the first D residue and the backbone carbonyl of the second), which is required for activity. In Motif II, **S/TXX**, the conserved serine or threonine is involved in hydrogen bonding to the phosphoryl oxygen. Motif III, **K(X)₁₈₋₃₀(G/S)(D/S)XXX(D/N)**, is involved in phosphoryl oxygen hydrogen bonding and coordination of the magnesium ion.^{3,4}

Several HAD member structures, including a calcium pump ATPase from rabbit,⁵ β -Phosphoglucomutase (PGM) from *Lactobacillus lactis*,⁶ YrbI (a 3-Deoxy-D-manno-octulosonate 8-phosphatase) from *Haemophilus influenzae*,^{7,8} phosphonoacetaldehyde hydrolase (PhnX) from *Bacillus cereus*,⁹ L-2 Haloacid Dehalogenase (L2H) from *Pseudomonas* sp. YL,¹⁰ TM0651 (a putative carbohydrate phosphatase) from *Thermotoga maritima*,¹¹ human mitochondrial deoxyribonucleotidase (HMD),¹² and a recently identified phosphoglycolate phosphatase (PGP) from *Thermoplasma acidophilum*¹³ have been solved by X-ray crystallography. Phosphoserine phosphatase (PSP) from is the most extensively studied of the HAD phosphatases, with its reaction pathway having been mapped out crystallographically (*Methanococcus jannaschii*).^{4,14} All the HAD structures reveal a hydrolase domain consisting of an α/β Rossmann fold that brings the conserved motifs together in the active-site. The structures also reveal inserted or “cap” domains of divergent sequences and sizes that confer

The atomic coordinates and structure factors in this study have been deposited in the Protein Data Bank, Research Collaboratory for Structural Bioinformatics, Rutgers University, New Brunswick, NJ (<http://www.rcsb.org/>) (codes 1RLM, 1RLO, and 1RLT.)

Abbreviations: MAD, multiwavelength anomalous dispersion; PEG, polyethylene glycol; SeMet, selenomethionine; HAD, haloacid dehalogenase; AMP, adenosine monophosphate

Grant sponsor: National Institutes of Health; Grant numbers: GM 62163 and GM050860.

*Correspondence to: David E. Wemmer, Department of Chemistry, University of California, Berkeley, CA94720. E-mail: DEwemmer@lbl.gov

Received 29 March 2004; Accepted 20 May 2004

Published online 18 January 2005 in Wiley InterScience (www.interscience.wiley.com). DOI: 10.1002/prot.20267

specificity on the enzymes and result in the diverse substrate range.^{1,4,9}

An analysis of the size and placement of these cap domains reveals three distinct classes.¹ The first includes proteins that contain an inserted domain after Motif I, the second includes a large inserted domain after Motif II, and the third contains little to no inserted domain. PSP, β -PGM, and HMD belong to the first class and all the structures reveal an inserted domain composed of a 4 or 5 helix bundle.^{6,12,14} Several proteins have been identified as belonging to the second class, including trehalose and sucrose phosphatases and two proteins, TM0651 and PGP, for which structures have recently been solved.^{11,13} The third class has the fewest members and includes histidinol phosphatase and magnesium dependent kinase I.¹ Despite the classification of hundreds of proteins as putative HAD phosphatases, the physiological functions of few have been pinpointed.

The genome of *Escherichia coli* K12-MG1655 (*E. coli* K12) provides the best available backdrop with which to investigate the global function of one of these uncharacterized HAD phosphatases. It is the best-characterized organism in terms of genomic annotation, the mapping of its metabolic and biosynthetic pathways, and an understanding of the elements that govern transcriptional regulation. Numerous centers are devoted to the systematic classification and functional annotation of every gene (PEC, <http://www.shigen.nig.ac.jp/ecoli/pec>, <http://www.genome.wisc.edu/>, Ecogene, <http://bmb.med.miami.edu/Ecogene/EcoWeb>, Ecocyc <http://www.ecocyc.org/>, RegulonDB).^{15–18} HAD phosphatases also appear to be particularly abundant in bacteria. *E. coli* K12 contains at least 9 of the type II class, with only one, *otsB*, a trehalose phosphatase, having an experimentally verified function¹⁹ (<http://www.shigen.nig.ac.jp/ecoli/pec>).

Here we report the characterization of the gene product from *E. coli ybiV* (b0822). YbiV belongs to the typeII class of HAD proteins, contains the conserved HAD motifs, and is a HAD phosphatase. We have investigated its function and mechanism using crystallographic, biochemical, and bioinformatics tools. In particular, we have solved the structure of YbiV in complex with beryllium fluoride (BeF_3^-) and aluminum fluoride (AlF_3), as stable mimics of the phosphorylated intermediate and transition state for hydrolysis, respectively. In both PSP and the bacterial receiver domains CheY and NtrC (related to HAD proteins by circular permutation), the BeF_3^- adduct has been shown to closely resemble the phospho-protein intermediate, binding occurring in the active-site in a geometry similar to the phosphoryl group.^{4,20}

MATERIALS AND METHODS

Materials

Oligonucleotide primers for constructing the non-his-tagged YbiV were purchased from Operon (Emeryville, CA). The Enzcheck Phosphate Assay (Molecular Probes, Eugene, OR) was used for kinetic studies. Reagents for cloning were purchased from New England Biolabs (Beverly, MA), Novagen (Madison, WI), or Invitrogen (La Jolla,

CA). Other materials for expression, purification, and crystallization were purchased from Sigma (St. Louis, MO), Amersham Biosciences (Arlington Heights, IL), and Qiagen (Chatsworth, CA).

Cloning

The his-tagged construct of YbiV was created by insertion of the gene (obtained by PCR amplification of *E. coli* K12) into the pRSETA vector (Invitrogen) between the BamHI and HindIII sites. Crystallization of the his-tagged YbiV did not yield high-quality crystals. A non-his-tagged construct was cloned into a pET21d vector (Novagen). The NcoI site in pET21d resulted in a serine to alanine mutation at position 2. A single base mutation in the region covered by the reverse primer resulted in a serine to tyrosine mutation at residue 267. This mutation occurs after the last helix in YbiV and is 3 residues from the end of what could be visualized in the electron density map. Both structural comparisons and the retention of para-nitrophenyl phosphatase activity indicated this mutation did not significantly affect the structure or activity of the protein. All the reported activity assays were performed on the his-tagged construct of YbiV, which contained the published sequence in addition to the histidine tag.¹⁵

Expression and Purification

The his-tagged construct was expressed in BL21(DE3) cells grown overnight at room temperature and purified by Ni-NTA agarose according to the Qiagen procedure. The pET21d construct was expressed in BL21(DE3) containing the plasmid pACYC. Expression was induced by addition of 1 mM IPTG at an O.D. of 0.6–0.8. The cells were grown overnight at 37°C and harvested by centrifugation. The cells were resuspended in 50 mM Tris, pH 8.0, 50 mM NaCl, 1 mM DTT, and 200 μM PMSF, lysed by sonication and centrifuged. The resulting supernatant was applied to a DEAE column, and the flow through applied to a Q column (Amersham Biosciences). Both columns were pre-equilibrated with 50 mM Tris, pH 8.0, 25 mM NaCl. The flow through from both columns was concentrated and applied to a Sephadex-75 sizing column in 50 mM Tris, pH 8.0, 500 mM NaCl, 1 mM EDTA, and 0.02% NaN_3 . The purified protein was dialyzed against 50 mM Tris, pH 7.4, 100 mM NaCl, and 1 mM DTT, and concentrated to ~20 mg/ml. Glycerol was added to 5%. Selenomethionine-containing protein was grown according to published procedures and treated the same as native protein.²¹

Crystallization and Data Collection

Crystals of YbiV were obtained using the hanging drop method. For the “native” protein (referred to henceforth as protein crystallized without beryllium or aluminum fluoride), 2 μl of concentrated protein solution were mixed with 2 μl of reservoir solution, which contained 0.1M cacodylic acid (pH 5.3), 0.2 M sodium acetate, and 15 % (w/v) PEG 8k. Large crystals appeared within hours. For AlF_3 and BeF_3^- derivatized protein, MgCl_2 was added to the protein solution to 5 mM Mg^{2+} and allowed to incu-

TABLE I. Data Collection Statistics

Dataset	Native	BeF ₃ ⁻	AlF ₃	λ1 (MAD)	λ2	λ3
Wavelength (Å)	1.000	1.000	1.000	.97872	.97890	.96373
Space group	P2 ₁ 2 ₁ 2 ₁	P2 ₁ 2 ₁ 2 ₁	P2 ₁ 2 ₁ 2 ₁	P2 ₁ 2 ₁ 2 ₁		
Unit cell (Å)						
a	71.82	72.28	71.76	72.05		
b	91.60	91.19	91.17	91.76		
c	186.56	176.41	183.85	187.02		
Resolution (Å)	(20–1.9)	(50–2.0)	(50–2.2)	(20–2.8)	(20–2.8)	(20–2.8)
Completeness ^b	98.6 (98.3)	100 (100)	99.7 (100)	98 (92.8)	98 (94)	97 (93)
I/σ	23.5 (4.5)	35 (13)	31 (5)	18 (4.7)	19 (6.3)	16 (3.6)
R _{sym} (%) ^a	7.6 (22.4)	11.2 (10.8)	8 (25)	12.4 (55.6)	10.6 (38.5)	12.4 (65.9)
Unique refl.	96,340	78,528	61,606	30,807	30,668	30,741

^aR_{sym} = Σ|I_i - ⟨I_i⟩|/ΣI_i.^b(-) indicates last shell.

bate, while BeCl₂ or AlCl₃ were combined with a 5× molar excess of NaF. These mixtures were added to the protein solution to a final concentration of 2 mM. Crystals formed under the same conditions as the native protein but appeared in a couple of days. Selenomethionine-derivatized protein crystallized under the same conditions but at higher PEG concentration (18%). Glycerol was used as a cryoprotectant (added to a final concentration of 20%) and the crystals were flash frozen in liquid nitrogen before data collection. All crystals belonged to the space group P2₁2₁2₁ had similar cell dimensions, and contained 4 protein molecules per asymmetric unit (see Table I).

All data were collected at the Advanced Light Source on Beamlines 5.0.2 and 8.3.1. These beamlines are equipped with ADSC Quantum4 CCD Detectors. Data processing and scaling were carried out using HKL2000, DENZO, and SCALEPACK.²²

Structure Determination

The structure of YbiV was initially solved using three wavelength MAD data from selenomethionine derivatized protein, from crystals that diffracted to 2.8 Å. The protein sequence contains 8 methionines and 32 sites were expected based on four monomers per asymmetric unit. Twenty-five of the 32 sites were found by the program SOLVE and refined using the program SHARP.^{23,24} The native and SeMet data were merged with the phases found from SOLVE and the program RESOLVE was used to improve the phase, for automated model building, and density modification.^{25,26} The model produced by RESOLVE was largely complete and was fully completed by manually adding residues according to the 2F_o-F_c density map produced by the program CNS, and visualized using the program O.²⁷ After model building, the structure was refined against the native data using the program CNS.²⁸ Non-crystallographic symmetry (NCS) averaging was employed until the final stages of refinement, when the NCS restraints were relaxed and each molecule was refined individually. For the AlF₃ derivatized protein, the native structure was used as a starting model and refined against the AlF₃ reflections using CNS. Any differences in the structures were adjusted manually to fit the AlF₃ 2F_o-F_c

map, including the placement of aluminum fluoride in the active-site. For the BeF₃⁻-derivatized protein, the molecular replacement protocol in CNS found three of the molecules and the fourth molecule was located manually after some refinement and examination of the 2F_o-F_c map. Refinement of the structures was carried out by manual adjustment followed by minimization using CNS. Ordered water molecules were picked using an automated script in CNS and then manually inspected.

Structure Analysis and Representation

Analysis of the structure quality was done using procheck from the CCP4 suite of programs.²⁹ Figures were made using Molscript, Raster3D, and Pymol.^{30–32}

Phosphatase Assays

The ability of his-tagged YbiV to catalyze the dephosphorylation of various compounds was measured using the Enzchek Phosphate Assay (Molecular Probes) adapted to a 96-well plate format. YbiV reactions were carried out in plate wells at room temperature in a total volume of 50 μL. Reactions were initiated by addition of substrate (15 mM) to a solution containing YbiV (0.024–3.0 μM) in 50 mM MES, pH 5.4, 10 mM MgCl₂. After 30 min, 200 μL of quench/assay reagent [270 mM Tris, pH 7.5, 27 mM EDTA, and Enzchek assay components MESG (270 μM) and purine nucleoside phosphorylase (1.5 U/mL)] were added and mixed by repeated pipetting. For each substrate, a control reaction lacking YbiV was run in an identical fashion. Each plate also contained phosphate standards (0–300 μM in 50 μL reaction buffer). After 15-min incubation with quench/assay reagent, absorbances at 360 nm were read using a Molecular Devices Spectramax 340 plate reader. For each substrate, the rate of YbiV-dependent phosphate release was the difference between the rate for the YbiV-containing reaction and the control lacking YbiV. For all except the lowest activity substrates (P-Ser, P-Thr, P-creatine, and ATP), the product absorbance was far above background. For several substrates, substrate concentration was varied (1–50 mM) and double reciprocal plots used to deduce K_m and k_{cat} values.

TABLE II. Phasing and Refinement Statistics

Resolution range (20–2.8 Å)	Phasing			
	Peak	Edge	Remote	All
<i>R</i> _{cullis} (iso) ^a		0.633	0.738	
<i>R</i> _{cullis} (ano) ^b	0.612	0.682	0.739	
FOM (acen/cen)				0.67/0.43
Dataset	Refinement			
	Native	BeF ₃ [−]	AlF ₃	
Resolution range (Å)	(20–1.9)	(20–2.0)	(20–2.2)	
No. of reflections used				
Working	85,387	69,583	53,778	
Test	9,467	7,797	6,059	
<i>R</i> -value (%) ^c	21.9	21.9	22.1	
Free <i>R</i> -value (%)	24.8	25.1	26.4	
Completeness (%) (highest shell)	97.1 (94.9)	98.6 (97.2)	96.5 (90)	
Sigma cutoff	0.0	0.0	0.0	
RMS deviations from ideal				
geometry				
Bond length	0.006	0.008	0.009	
Angle (°)	1.6	1.5	1.8	
Dihedral (°)	23.1	23.1	23.2	
Improper (°)	0.99	1.06	1.22	
Temperature Factors (Å ²)				
Protein atoms	29.2	25.3	40.9	
Solvent	46.9	49.8	42.2	
No. of atoms				
Protein	8,536	8,532 ^d	8,516	
Water	577	454	396	
Mg ²⁺	4	4	4	
Other	36	12	32	
Ramachandran plot stats (%)				
Most favored	88.2	88.3	88.4	
Other allowed	11.8	11.7	11.6	

^a*R*_{cullis} (iso) = $\sum |\Delta_{\text{iso}}(\text{obs}) - \Delta_{\text{iso}}(\text{calc})| / \Delta_{\text{iso}}(\text{obs})$ for centric reflections.

^b*R*_{cullis} (ano) = $\sum |\Delta_{\text{ano}}(\text{obs}) - \Delta_{\text{ano}}(\text{calc})| / \Delta_{\text{ano}}(\text{obs})$ for acentric reflections. $\Delta_{\text{ano}}(\text{obs})$ is the anomalous difference.

^c*R*-value = $\sum |F(\text{obs}) - F(\text{calc})| / \sum F(\text{obs})$.

^d(includes BeF₃[−] atoms as part of new residue).

RESULTS AND DISCUSSION

Quality of the Models

The structures of the native BeF₃[−] and AlF₃ bound YbiV were refined to 1.9, 2.0, and 2.2 Å, respectively, with pdb accession codes 1RLM, 1RLO, and 1RLT. Statistics for the data collection and refinement are given in Tables I and II. All the models were complete except for the first and/or second residues, and the last residue. Regions of higher B-factors were located around loops (residues 151–161), and in turns (residues 178–181), and at the termini, depending on crystallographic contacts present for a particular molecule in the asymmetric unit. The final models included magnesium ions, glycerol molecules, and water molecules. Beryllium or aluminum trifluoride was clearly visualized in the active-sites of those protein molecules whose crystallization buffers contained those additives.

Overall Structure and Structural Comparisons

The crystal structure of YbiV reveals a two domain protein, the characteristic hydrolase domain with an α/β

Rossmann fold, and an α/β domain corresponding to the inserted domain [Fig. 1(A,B)]. At the interface of the two domains is the active-site, which forms a negatively charged cavity [Fig. 1(D)]. The hydrolase domain consists of a 6-stranded parallel β sheet surrounded by 6 α helices. The sheet is extended by a β hairpin, the end of which leads to the inserted domain. The inserted domain occurs between Motifs II and III (as expected from sequence analysis) and extends from residues 80–190. The inserted domain contains a 6-stranded mixed β sheet surrounded by 3 α helices.

The topology of YbiV is very similar to that of TM0651, which has an unknown function but is speculated to have carbohydrate substrate(s).¹¹ When the full structures of TM0651 and native YbiV are overlaid, the C α rmsd is ~ 1.85 Å, with the hydrolase domains appearing slightly offset. If the domains are detached and overlaid independently, the rmsd reduces to 1.6 Å for the inserted and 1.3 Å for the hydrolase domains. This indicates that there may be some flexibility in the relative domain orientation depending on the state of the protein, a trait attributed to other HAD phosphatases.^{4,13} More generally, the structures of these two proteins are probably representative of many of the type II class of HAD hydrolases, with specificity achieved by altering the composition of the residues that line the inserted domain.

A search for structurally similar proteins on the DALI server yielded many other HAD hydrolases and proteins that contain the Rossmann fold.³³ The proteins with the highest Z-scores were YrbI and PSP. Despite differences in the placement, size, and topology of the cap domains, the hydrolase domains of YbiV, YrbI, and PSP overlay with an rmsd of 1.5 Å, reflecting the strong structural conservation of this domain among HAD proteins [Fig. 1(C)].^{7,14}

Inserted Domain and Substrate Binding

In all 4 monomers of the native YbiV crystals, at least one glycerol molecule is bound in the inserted domain in a hydrophilic cavity, forming several hydrogen bonds with residues that line the cavity. This is likely the binding pocket for the true substrate. Hydrogen bonds to the glycerol hydroxyls originate from inserted domain residues Tyr 130, Ser 150, Ser 178, and Asp 184, and hydrolase domain residues Asn 46 (Motif II) and Asn 68 [Fig. 2(A)]. Lys 148 forms the back of the cavity, hydrogen bonding to the carbonyl of Gly 45 (Motif II) and forming a salt bridge with Glu 67. These residues line both sides of the cavity and suggest that a substrate with several polar groups is most likely to bind in it.

As in native crystals, there are 4 molecules per asymmetric unit in the AlF₃ and BeF₃[−] bound structures. In each of these, two molecules very closely resemble the native structures, including the glycerol molecule bound in the inserted domain. In the other two molecules in each case, however, Phe 180 in the turn between strands 10 and 11 shifts over to stack against His 129, effectively closing off the inserted domain pocket. This shift tilts helix 5 out and slightly changes

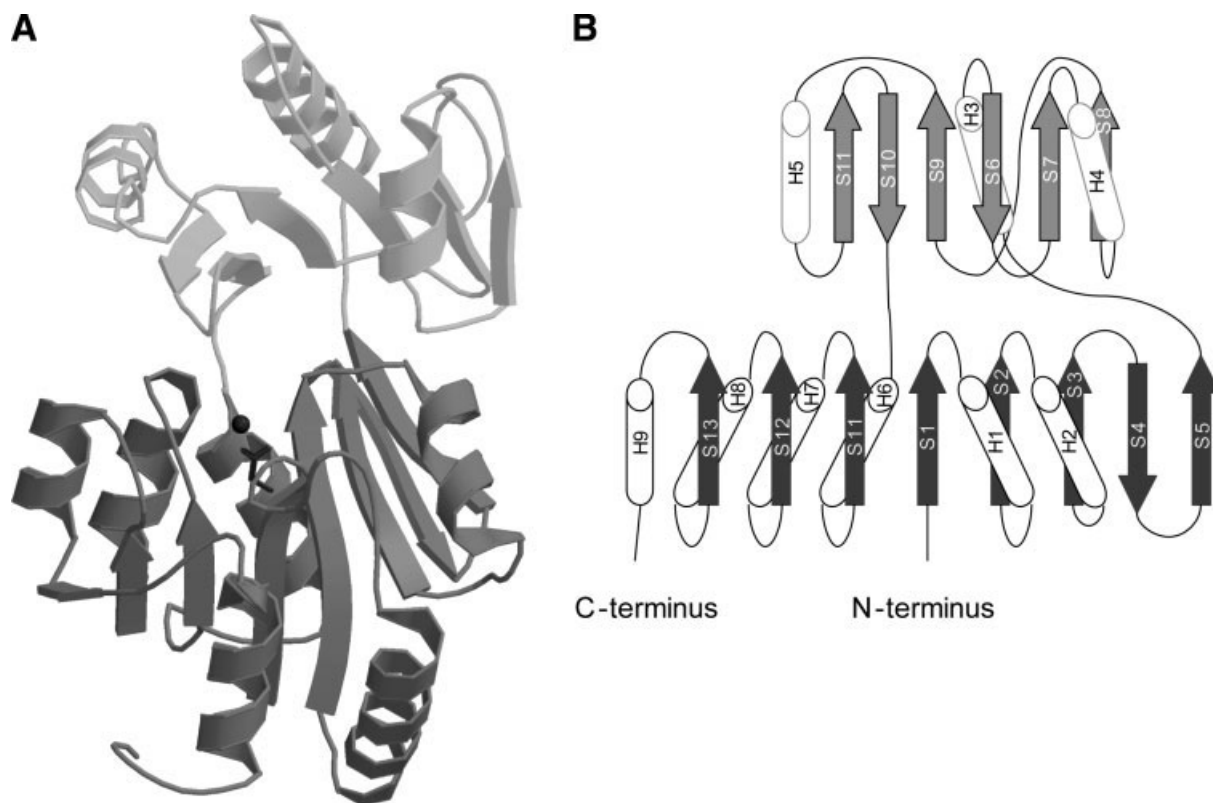


Fig. 1. **A:** Ribbon diagram of the structure of YbiV. The hydrolase domain is colored in medium grey, the inserted domain in light grey. The nucleophilic aspartate and the magnesium ion are dark grey. **B:** Secondary structure topology of YbiV shaded similarly to A. **C:** Overlay of the hydrolase domains of PSP (pink) and YrbI (blue) onto the full structure of YbiV (grey), all as alpha carbon backbones. The full structures of the PSP and YrbI monomers (top and bottom, respectively) are shown to the right as ribbons. **D:** Surface potential plot of YbiV. Acidic regions are shown in red, basic regions in blue. (Fig. 1 continued on next page.)

the orientation of strands 10 and 11 but otherwise leaves the structure unperturbed [Fig. 2(B)]. This stacking interaction may be a means of preventing substrate from binding while the protein is phosphorylated. Analogously, a flexible hinge and disordered loop in PSP clamp over the active-site in the phosphorylated, substrate and product-bound states.⁴

Active-Site Architecture

Native active-site

A common feature of HAD phosphatases is the negatively charged environment of the active-site.^{11,13} In each of the native, beryll fluoride, and aluminum-fluoride bound structures of YbiV, this negative charge is tempered by the presence of a magnesium ion and several ordered water molecules that form an extensive hydrogen bonding network. For the native YbiV, no additional magnesium was added to the protein purification or crystallization buffers, indicating the ion co-purified with the protein.

In the native structure, the Mg^{2+} ion is hexacoordinate with Asp 9 (the site of phosphorylation), the carbonyl of Asp 11 (Motif I), Asp 215, Ser 216 (Motif III), and watA and watB [Fig. 3(A)] as ligands. Lys 192 forms a salt bridge with Asp 219 (Motif III) (2.5 Å). Wat C hydrogen bonds to the carboxyl of Asp 11 while watD bridges Asp 9 and Ser 44 (Motif II.) As might be expected from sequence and struc-

tural conservation, the active-sites of HAD phosphatases are highly superimposable. Despite differences in sequence around Motif III, the active sites of magnesium-bound YbiV and cobalt-bound YrbI superimpose well [Fig. 3(B)].⁷

BeF₃⁻-bound active-site

Both response regulators and HAD phosphatases share the Rossman fold and use an active-site aspartate as the site of phosphorylation. In the response regulators NtrC and CheY, beryll fluoride (BeF₃⁻) has been shown to bind the active-site aspartate in a tetrahedral geometry similar to the phosphoryl group. Functional studies indicate that BeF₃⁻ binding induces the same conformational changes as phosphorylation and leads to downstream signaling.²⁰ This indicates that BeF₃⁻ both structurally and functionally mimics the phosphorylated state. Among HAD phosphatases, BeF₃⁻-bound structures have been solved for both PSP and HMD in an effort to better understand their reaction pathways.^{4,12}

The 2F_o-F_c map of the beryll fluoride-bound active-site of YbiV reveals density corresponding to the 3 fluorines, which, together with O2 of Asp 9, form a tetrahedral structure around the beryllium [Fig. 4(A)]. The magnesium ion is coordinated by F1, the carbonyl of Asp 11, Asp 215, watA, watB (which mediates coordination by both Ser

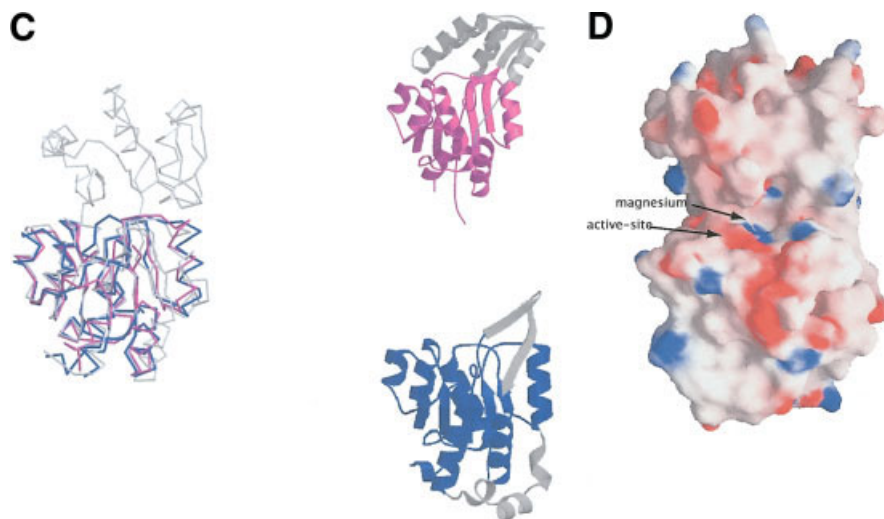


Figure 1. (Continued.)

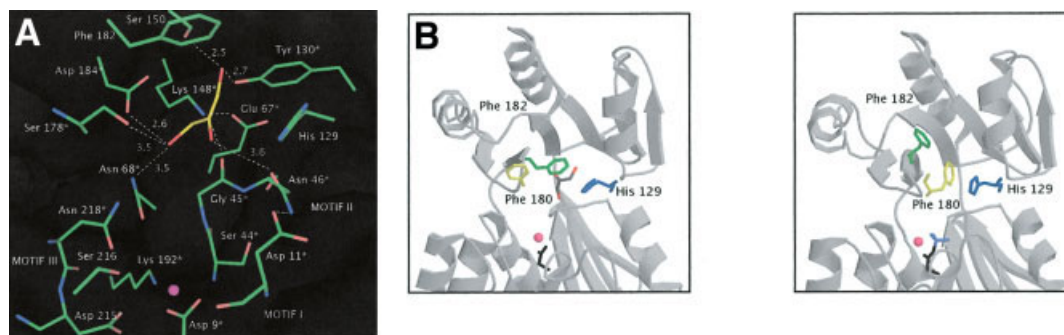


Fig. 2. **A:** Glycerol binding in the inserted domain. The glycerol is represented in yellow, the protein in green. The HAD motifs are labeled. Hydrogen bonds are represented by white dashed lines with the respective distances labeled above (in Angstroms). Residues with an * are conserved among the closest homologs to YbiV. **B:** Differences in conformation of the inserted domain in the native glycerol bound YbiV (**left**), and the non-glycerol bound BeF_3^- YbiV (**right**). In the absence of glycerol, Phe 180 shifts over to stack against His 129, closing off the binding pocket. The glycerol is shown in grey and red, the magnesium ion, magenta, and the berylliofluoride (**right**) in purple.

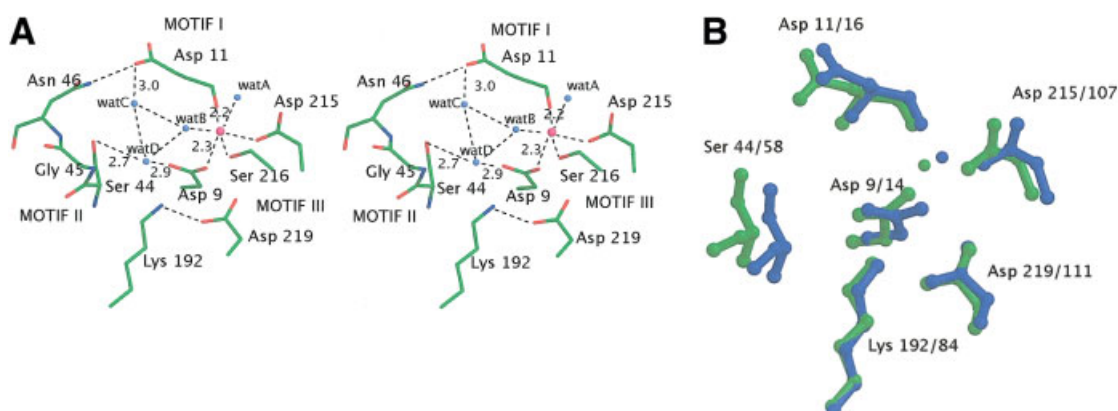


Fig. 3. **A:** Stereoview of the native active-site of YbiV. The magnesium ion is represented by a magenta sphere, water molecules as blue spheres. Hydrogen bonds are represented as dashed lines and numbers indicate distances in Angstroms. The active-site motifs are labeled. **B:** Overlay of the active-sites of YrbI from *H. influenzae* (green) and YbiV (blue.) The blue sphere represents magnesium, the green sphere, cobalt. The residue numbers are labeled, YbiV on the left, YrbI on the right.

216 and Asn218), and Asp 9. F2 forms long hydrogen bonds to Lys 192 (2.80 Å), Asn 218 (3.00 Å) (Motif III), and the amide of Gly 45 (Motif II) (3.10 Å). F3 is hydrogen bonded

to Ser 44 (Motif II) (2.60 Å). WatC, coordinated by the carbonyl of Ser 178 from the inserted domain and the carboxyl of Asp 11 (2.70 Å), is collinear with both the

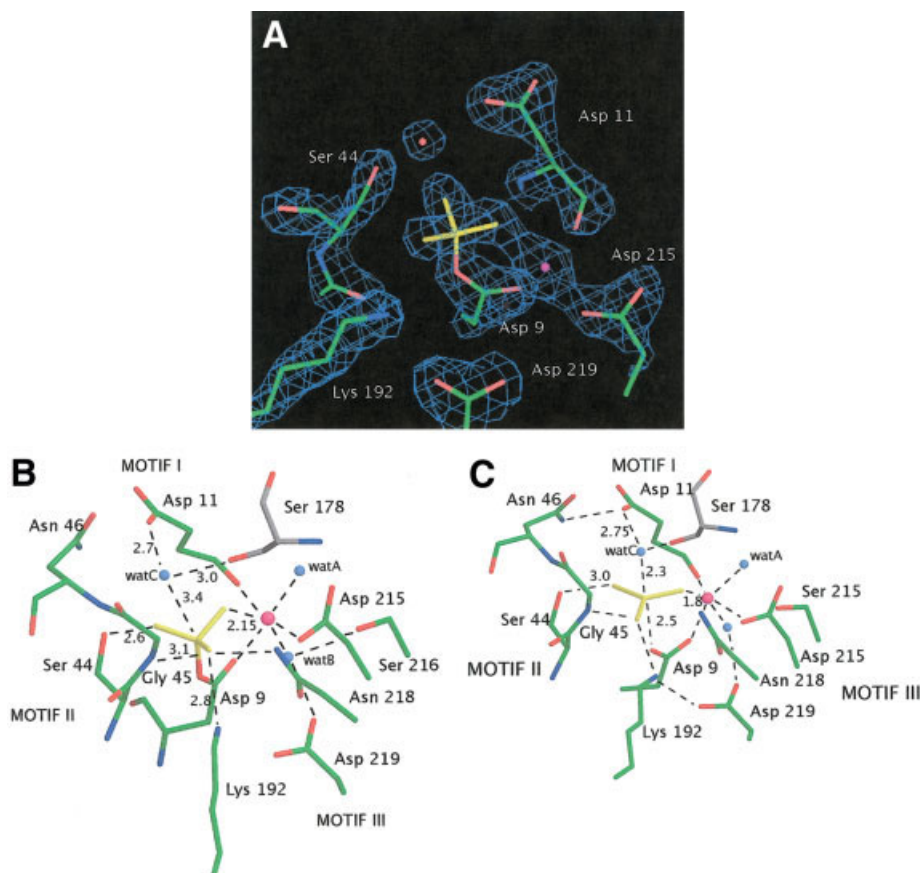


Fig. 4. **A:** 2F_o-F_c electron density map of the BeF₃⁻ bound active-site of YbiV. The magnesium is colored in magenta, water in red, and the berylliofluoride in yellow. **B:** Stick diagram of the active-site of beryllio-fluoride bound YbiV. The beryllium and fluorines are represented in yellow, the active-site motifs in green, and Ser 178, from the inserted domain, in grey. Nitrogens and oxygens are blue and red, respectively. Dotted lines represent hydrogen bonds, with the corresponding distances labeled in Angstroms. Water molecules are represented by blue spheres, the magnesium ion by a magenta sphere. **C:** Stick diagram of the aluminum fluoride bound active-site of YbiV. The aluminum fluoride is represented in yellow. Colored similarly to B.

beryllium and O2 of Asp 9 at a distance of 3.50 Å [Fig. 4(B)]. This active-site geometry is very similar to that seen in the BeF₃⁻-bound active-site of PSP. As in that structure, watC is in an ideal position to act as the hydrolytic water molecule, activated by the carboxylate of Asp 11, which acts as a base.⁴

AlF₃-bound active-site

The AlF₃-bound active site is very similar to that with the BeF₃⁻-bound site [Fig. 4(C)]. The hydrogen bond distance between Ser 44 and F2 has increased slightly from 2.6 to 3.0 Å. The largest changes occur around the aluminum fluoride. The distance from O2 of Asp 9 to the aluminum increases while the distance from watC to the aluminum has shortened significantly (from 3.4 to 2.3 Å.) This reflects the intermediate (planar) state of the phosphoryl group as it is hydrolyzed and agrees well with a recent structure that trapped a putative pentavalent phosphate intermediate of phospho-glucumutase (though an alternative explanation of the density as MgF₃⁻ has been proposed).^{34–36}

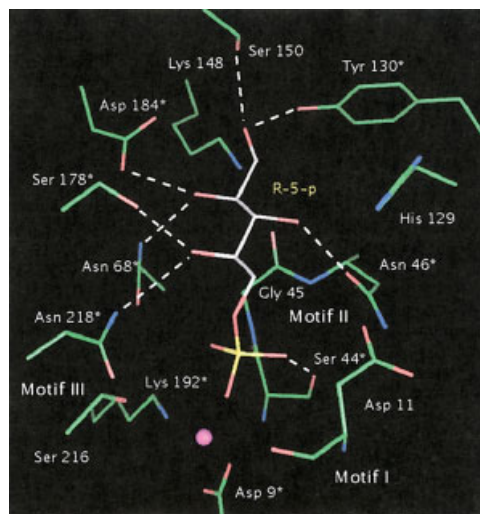


Fig. 6. Ribose-5-phosphate (grey), the best performing substrate, modeled into the inserted domain of YbiV. The magnesium ion is represented by a magenta sphere.

Mechanism

The structure of YbiV in its native, BeF_3^- - and AlF_3 -bound forms suggests that YbiV shares a similar mechanism for phosphotransfer as the best-characterized HAD phosphatase, PSP. The YbiV structures all contain the physiologically relevant Mg^{2+} ion that orients the HAD active-site motifs and facilitates subsequent binding of the phosphate group of the substrate. The binding of one or more glycerol molecules in the inserted domain reveals the substrate binding pocket, which is hydrophilic in nature. When the substrate is properly oriented in the active-site, Asp 9 nucleophilically attacks the phosphate group, which results in protein phosphorylation. The phosphorylated intermediate is stabilized by coordination by Lys 192 (motif III), the amide of Gly 45 (motif II), and Mg^{2+} . At this point, the substrate likely acquires a proton either from a water molecule or a residue in the active-site and is released. In the absence of substrate, Phe 180 shifts over to stack against His 129 on the opposite side of the inserted domain. This effectively closes off the substrate binding pocket while the protein is phosphorylated. A water molecule coordinated by the carbonyl of Ser 178 and the carboxylate of Asp 13 likely acts as the hydrolytic molecule after having a proton extracted by Asp 13. This is supported by the BeF_3^- - and AlF_3 -bound structures, which mimic the phosphorylated state of the protein and the transition state of hydrolysis, respectively.

Sequence Comparison

A PSI-BLAST search of YbiV yields hundreds of hits from putative HAD hydrolases.³⁷ The highest scoring sequences (from 99 to 51% identity) are from closely related organisms (*Salmonella typhimurium*, *Shigella flexneri*, other *E. coli* strains) and include another protein from *E. coli* K12, YbjI. A sequence alignment of YbiV with homologs of varying degrees of sequence similarity is shown in Figure 5.

Although many of the absolutely conserved residues in the alignment stem from the active-site-motifs, a careful inspection of the YbiV sequence alignment reveals that many of the residues lining the inserted domain are completely or strongly conserved among the closest homologs of YbiV (first 6 sequences in the alignment), indicating their potential functional relevance. These include residues N46, E67, N68, Y130, K148, S178, and D184, which are all involved in glycerol binding or structural integrity of the inserted domain (i.e., K148-E67 forming the back of the inserted domain cavity.) This suggests perhaps structurally similar substrates for these proteins. Although the two residues involved in the stacking interaction, Phe 180 and His 129, are not strictly conserved in the closest homologs, they are conserved as aromatic residues with YbjI from *E. coli* K12 as the lone exception.

The alignment also indicates factors that may alter substrate specificity. For instance, S150 of YbiV, which lines the inserted domain and forms a hydrogen bond to glycerol, is replaced by a glycine in YbjI, resulting in less hydrogen-bonding potential. After these highest scoring

hits come hundreds of other type II hydrolases from bacteria, ranging in sequence identity from 20–40% with YbiV. Most of these proteins are classified as belonging to the COF-subfamily of type II hydrolases, all predicted to have similar inserted domain topology to YbiV (family classifications: TIGR00099 www.tigr.org and IPR000150 www.ebi.ac.uk/interpro). Proteins belonging to this subfamily are almost exclusively present in bacteria. *E. coli* K12 has 6, *Listeria monocytogenes* EGD-e has 12, *Lactococcus lactis* subsp. *lactis* has 8, and so on. The COF-subfamily is a subset of subfamily IIB (TIGR01484, IPR006379). Other subfamilies of IIB include trehalose-phosphatases, sucrose-phosphate phosphatases, eukaryotic phosphomannomutases, and YedP hydrolase (a putative mannosyl-3-phosphoglycerate phosphatase).³⁸ Connections between these subfamilies are evident in the albeit-lower scoring hits of the PHI-Blast search of YbiV, which include sucrose and trehalose phosphatases. The remaining four sequences in the alignment include sucrose phosphatase from maize,³⁹ trehalose phosphatase from *E. coli* K12, and Cof and YbhA, two of the remaining 4 predicted type IIB hydrolases from *E. coli* K12 (Fig. 5). It is clear that YbiV is more distantly related to these proteins. However, the overall homology in the placement of the motifs and sequence length is quite strong, indicating their structures are likely similar. Gaps in sequence, corresponding to secondary structure in the inserted domain, may indicate differences in the inserted domain topology, particularly for sucrose and trehalose phosphatases.

Catalytic Activity

Potential substrates for YbiV were tested in *in vitro* assays and ranked according to the rate at which inorganic phosphate (Pi) was released relative to the best substrate tested (Table III). YbiV had negligible activity towards phosphoserine, phosphothreonine, and phosphocreatine, some of the first substrates tested. The hydrophilic nature of the inserted domain (as revealed by the structure and bound glycerol) led us to try substrates with several polar groups. Glycerol-1-p and glycerol-2-p were hydrolyzed appreciably, with glycerol-1-p being hydrolyzed slightly faster. The best substrates in our test panel were ribose-5-p and glucose-6-p. Other sugar molecules, including 2-deoxy-glucose-6-p, mannose-6-p, and fructose-6-p, are hydrolyzed appreciably, further indicating a terminal sugar phosphate as a likely candidate for the substrate. Sucrose-6-p and glucose-1-p hydrolyzed very poorly in comparison to the other substrates. Sucrose-6-p is a two-ringed sugar molecule that is too large to be accommodated in the active-site. Though glucose-1-p is also a terminal sugar phosphate, steric clashes made by placing C6 towards the top of the inserted domain may prevent it from being hydrolyzed. The other possible explanation is that this molecule cannot ring open to a linear form, as opposed to glucose-6-p and ribose-5-p, which can. Particularly in their linear forms, these molecules fit nicely into the active-site, with approximately the correct length necessary to reach Asp 9 and form hydrogen bonds on either side of the cavity (Fig. 6). This suggested to us a linear sugar as a candidate

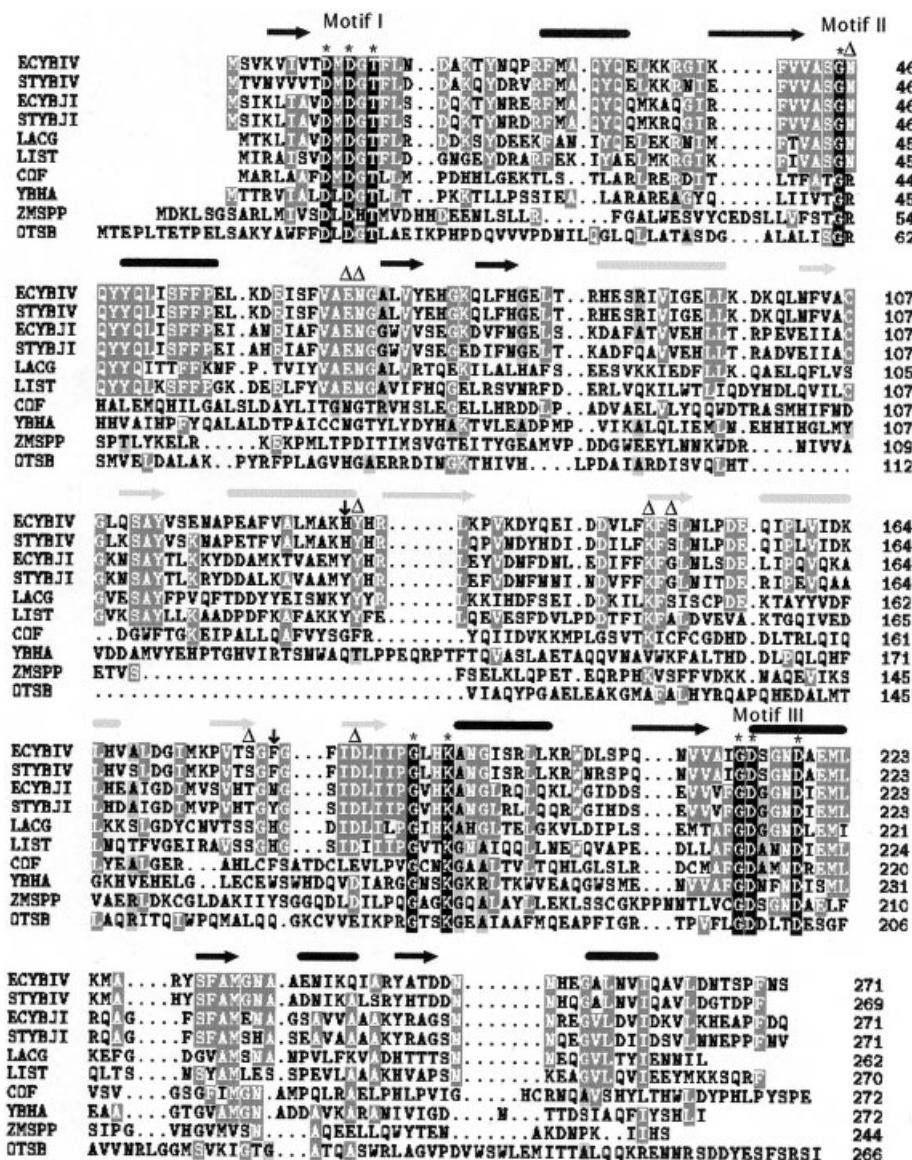


Fig. 5. Sequence alignment of YbiV and its homologs, YbiJ from *E. coli*, EcyBJI-P75809, YbiV and YbiJ from *Salmonella typhimurium* (STYBIV-CAD05288 and STYBJI-AAL19778), and proteins from *Lactobacillus gasseri* (LACG-ZP_00046022), *Listeria monocytogenes* (LIST-NP_463949), cof (NP_414980) and YbhA (NP_415287) from *E. coli* K12, sucrose phosphatase from maize (ZMSPP), and trehalose phosphatase (otsB, NP_416411) from *E. coli*. One hundred seventy-nine residues are omitted from ZMSPP for clarity. Fully conserved residues are white with black background, conserved are white with dark grey background, and all other residues are white with light grey background. The secondary structure for the hydrolase domain (black) and inserted domain (grey) is indicated over the alignment. Triangles represent the residues involved in glycerol binding and/or line the inserted domain cavity. Arrows indicate the residues involved in the stacking interaction. Figure made with Texshade.⁵⁰

for the substrate, though glucose-6-p and ribose-5-p are predominantly in their cyclized form in solution. Although 6-p-gluconate is linear, it hydrolyzed poorly, which may reflect the inability of the inserted domain to accommodate a molecule with a negative charge due to electrostatic repulsion with Asp 184. Sorbitol-6-p, which is linear and differs from glucose-6-p only in the replacement of a carbonyl oxygen with a hydroxyl, was also appreciably hydrolyzed, though about 5 times less rapidly than the

best substrate, ribose-5-p. Thus, a cyclic sugar cannot be definitively ruled out as a possible substrate.

The kinetic constants (k_{cat} and K_m) were analyzed for ribose-5-p, glycerol-1-p, and glycerol-2-p (Table III). We observe values for K_m and k_{cat} ranging from approximately 4–6 mM and 1–4 s⁻¹, respectively. This is very similar to the range of kinetic constants observed when YrbI from *H. influenzae* was first tested for phosphatase activity.⁷ However, a later study, which isolated 3-deoxy-d-

TABLE III. Activity of YbiV Towards a Variety of Potential Substrates.[†]

Phosphatase activity of YbiV		
Substrate	V/[E](s ⁻¹)	% Ribose-5-p
Ribose-5-p	2.4	100.0
Glucose-6-p	1.5	62.5
Glycerol-1-p	0.59	24.6
2-deoxy-glucose-6-p	0.54	22.5
Mannose-6-p	0.48	20.0
Sorbitol-6-p	0.47	19.6
Glycerol-2-p	0.47	19.6
Fructose-6-p	0.37	15.4
p-tyr	0.033	1.4
6-p-gluconate	0.031	1.3
Sucrose-6-p	0.0097	0.4
p-ethanolamine	0.0069	0.3
Glucose-1-p	0.0057	0.2
ATP	0.0013	0.1
p-ser	0.0004	0.0
p-thr	0.0012	0.1
p-creatine	0	0.0

Kinetic constants		
	k _{cat} (s ⁻¹)	K _m (mM)
Glycerol-1-p	0.9	6
Glycerol-2-p	0.5	4.5
Ribose-5-p	4	6

[†]The first column, V/[E], is velocity ($\mu\text{MP}_i/\text{s}$) divided by enzyme concentration. The second is the relative phosphatase rate vs. the best substrate, ribose-5-p. Kinetic constants for ribose-5-p and glycerol-1-p and glycerol-2-p are shown below the trial substrates.

manno-octulosonate 8-phosphatase activity from *E. coli* K12 (an activity previously unassociated with a specific gene) identified the source of activity as YrbI, with kinetic constants K_m and k_{cat} of 75 μM and 175 s^{-1} , respectively. These constants better reflect the high specificity typically associated with enzymatic activity.⁸ Although the likeliest interpretation of the kinetic data is that the physiological substrate of YbiV has not been found, the possibility still exists that some enzymes may be designed to have poorer binding and/or catalytic efficiency as a means of regulating activity.

Genomic Location and Functional Genomics

Often genes that are functionally related are grouped within the genome or belong to the same transcriptional unit or operon. For instance, *otsB*, the *E. coli* K12 gene for trehalose phosphatase, is in the same operon as *otsA*, the trehalose synthetase gene (<http://www.ecocyc.org/>). YbiV (b0822) is surrounded by genes that are seemingly diverse in nature, and is not predicted to form part of an operon (RegulonDB).¹⁸ Surrounding genes encode proteins that are annotated as putative ABC transporters (b0820), unidentified (b0821), pyruvate formate lyase (b0823), pyruvate formate lyase activator (b0824), and the start of the molybdenum uptake operon (b0826) (http://bayesweb.wadsworth.org/binding_sites).⁴⁰ Ten genes upstream is the *dps* gene (b0812), a global regulator under starvation conditions (www.ecocyc.org).¹⁷ While it has been shown

that genes of diverse functions may belong to the same operon, the above information does not provide many clues to the function of YbiV.⁴¹ We also looked at genomic location of genes with gene products of >20% sequence identity to YbiV (YigL, YbjI, Cof, YidA, YbhA). Many were in similarly diverse regions except for YbhA, the last gene in the molybdenum uptake operon. Interestingly, YbjI (b0844) (50% identity to YbiV) is located 22 genes downstream of YbiV, in a region with genes involved in the DEOR (deoxyribose) metabolic pathway (<http://www.shigen.nig.ac.jp/ecoli/pec>).

Another genomics-based tool for functional discovery is that of functional genomics. The two main approaches to functional genomics are monitoring expression levels of all genes in response to different external conditions, and making a knockout of each gene and determining the phenotype.^{42–44} The first type of experiment typically reports the ratio of mRNA transcripts present in response to growth conditions (different growth media, knockouts of transcription factors, regulators, stationary growth phase, etc.) compared to a control condition. Results under different conditions can be clustered to group genes that might be involved in related pathways. Although universal standards for the interpretation of DNA microarray data are not yet available, such experiments have already proven useful in identifying the cellular functions or pathways of proteins of unknown function.⁴⁵ The second approach assesses the ability of a knockout to grow on many different types of media (sugars, amino acids, etc.). Both the ability to grow and the speed at which the cells propagate can be monitored colorimetrically and can be compared to wild-type cells.⁴² This methodology has been validated by work on knockouts of “global regulators of carbon metabolism.” Systematic mutagenesis of every *E. coli* K12 gene is underway and each strain will be subjected to this type of analysis (<http://www.genome.wisc.edu/>). Series of multi-gene knockouts have already determined genes or regions required for *E. coli* survival, and these studies indicate that b0822 is not essential (<http://www.shigen.nig.ac.jp/ecoli/pec>).

In the case of YbiV, published microarray data have not revealed a condition in which expression of YbiV is greatly induced or suppressed. (Among homologous proteins, the protein YidA is slightly upregulated during growth on glucose.⁴⁶) Although access to unpublished “raw” microarray data is becoming increasingly available, it is difficult to judge how meaningful changes in expression are or define a “threshold” for up- or down-regulation without a full statistical analysis. Even so, unpublished, calibrated microarray data from www.genome.wisc.edu/functional.htm shows an increase in *ybiV* mRNA production upon mutation of the cAMP Receptor Protein, CRP (a ubiquitous cyclic AMP receptor and global regulator of secondary carbon metabolism).^{42,47,48} Further investigation reveals a CRP binding site 56 bp upstream from the start of *ybiV*, in a noncoding region⁴⁹ (http://arep.med.harvard.edu/ecoli_matrices/sco/crp.db). This combination of results suggests CRP is involved in the regulation of expression of

YbiV but it is difficult to glean more specific information from this finding.

The lack of significant enhancement or suppression of expression of YbiV has two possible explanations. The most obvious is that the proper conditions for the induction of expression have not yet been probed. The second is that the protein, for perhaps regulatory reasons, is constitutively expressed at low levels.

CONCLUSION

Mechanistic insights provided by the native, berylliofluoride, and aluminum-fluoride bound structures of YbiV, sequence homology, and biochemistry indicate that YbiV is a phosphatase with a sugar-like substrate. Although the physiological substrate could not be determined, the pronounced presence of homologous proteins in certain bacteria and absence in other branches perhaps indicate the sugars are unique to these organisms, or that the pathway involved is unique to these organisms, and not yet discovered. Since small molecules are generally present and metabolically active in their phosphorylated forms, this leads to the question of the functional significance of these reactions, whether they are regulatory (and perhaps active at some intrinsically low rate), involved in recycling of molecules, or induced by certain types of stress, less obvious than those that induce the synthesis of trehalose, for example. But, given the relatively close homology between the type II hydrolases present, it seems unlikely that these are non-specific phosphatases.

The combination of genomics, structural genomics, and functional genomics are complementary techniques. As in this case, structure and to some extent sequence analysis yielded a good indication of function, pinning down the nature of the reaction if not the specific substrate. This latter task may be much more difficult to achieve. Selective testing of compounds is useful in narrowing the range of possible substrates, but high-throughput techniques such as expression profiling and phenotypic analysis of gene knockouts may be increasingly important in both determining the cellular substrate and its importance in the metabolic pathways of the cell.

ACKNOWLEDGMENTS

We thank Ho Cho who was involved in the initial identification of YbiV as a potential phosphatase and Sydney Kustu for helpful discussions regarding the potential function of YbiV, and for access to some microarray data. Thanks also to Jeremy Glasner and the ASAP site at www.genome.wisc.edu for permission to cite microarray data available on their site. This work was supported by National Institutes of Health grants GM 62163 (to D.E.W.) and GM050860 (to R. Bourret).

REFERENCES

- Selengut JD. MDP-1 is a new and distinct member of the haloacid dehalogenase family of aspartate-dependent phosphohydrolases. *Biochemistry* 2001;40:12704–12711.
- Koonin EV, Tatusov RL. Computer analysis of bacterial haloacid dehalogenases defines a large superfamily of hydrolases with diverse specificity. *J Mol Biol* 1994;244:125–132.
- Collet J-F, Stroobant V, Pirard M, Delpierre G, Van Schaftingen E. A new class of phosphotransferases phosphorylated on an aspartate residue in an amino-terminal DXDX(T/V) motif. *J Biol Chem* 1998;273:14107–14112.
- Wang W, Cho HS, Kim R, Jancarik J, Yokota H, Nguyen H, Grigoriev IV, Wemmer DE, Kim S-H. Structural characterization of the reaction pathway in phosphoserine phosphatase: crystallographic “snapshots” of intermediate states. *J Mol Biol* 2002;319:421–431.
- Toyoshima C, Nakasako M, Nomura H, Ogawa H. Crystal structure of the calcium pump of sarcoplasmic reticulum at 2.6 Å resolution. *Nature* 2000;405:647–655.
- Lahiri SD, Zhang G, Dunaway-Mariano D, Allen KN. Caught in the act: the structure of phosphorylated *B*-phosphoglucomutase from *Lactococcus lactis*. *Biochemistry* 2002;41:8351–8359.
- Parsons JF, Lim K, Tempczyk A, Krajewski W, Eisenstein E, Herzberg O. From structure to function: YrbI from *Haemophilus influenzae* (HI1679) is a phosphatase. *Proteins* 2002;46:393–404.
- Wu J, Woodard RW. *Escherichia coli* YrbI is 3-deoxy-D-mannooctulosonate 8-phosphate phosphatase. *J Biol Chem* 2003;278:18117–18123.
- Morais MC, Zhang W, Baker AS, Zhang G, Dunaway-Mariano D, Allen KN. The crystal structure of *Bacillus cereus* phosphonoacetaldehyde hydrolase: insight into catalysis of phosphorus bond cleavage and catalytic diversification within the HAD enzyme superfamily. *Biochemistry* 2000;39:10385–10396.
- Hisano T, Hata Y, Fugii T, Liu J-Q, Kurihara T, Esaki N, Soda K. Crystal Structure of L-2-haloacid dehalogenase from *Pseudomonas* sp. YL: an α/β hydrolase structure that is different from the α/β hydrolase fold. *J Biol Chem* 1996;271:20322–20330.
- Shin DH, Roberts A, Jancarik J, Yokota H, Kim R, Wemmer DE, Kim S-H. Crystal structure of a phosphatase with a unique substrate binding domain from *Thermotoga maritima*. *Protein Sci* 2003;12:1464–1472.
- Rinaldo-Matthis A, Rampazzo C, Reichard P, Bianchi V, Nordlund P. Crystal structure of a human mitochondrial deoxyribonucleotidase. *Nature Struct Biol* 2002;9:779–787.
- Kim Y, Yakunin AF, Kuznetsova E, Xu X, Pennycooke M, Gu J, Cheung F, Proudfoot M, Arrowsmith CH, Joachimiak A, Edwards A, Christendat D. Structure and function-based characterization of a new phosphoglycolate phosphatase from *Thermoplasma acidophilum*. *J Biol Chem* 2003 Forthcoming. published online Oct. 10;pp. 42.
- Wang W, Kim R, Jancarik J, Yokota H, Kim S-H. Structure of phosphoserine phosphatase from *Methanococcus jannaschii*, a hyperthermophile, at 1.8 Å resolution. *Structure* 2001;9:65–71.
- Blattner FR, Plunkett G, Bloch CA, Perna NT, Burland V, Riley M, Collado-Vides J, Glasner JD, Rode CK, Mayhew GF, Gregor J, Davis NW, Kirkpatrick HA, Goeden MA, Rose DJ, Mau B, Shao Y. The complete genome sequence of *Escherichia coli* K-12. *Science* 1997;277:1453–1474.
- Rudd KE. EcoGene: a genome sequence database for *Escherichia coli* K-12. *Nucleic Acid Res* 2000;28:60–64.
- Karp PD, Riley M, Saier M, Paulsen IT, Paley S, Pellegrini-Toole A. The EcoCyc database. *Nucleic Acid Res* 2002;30:56–58.
- Salgado H, Santos-Zavaleta A, Gama-Castro S, Millan-Zarate D, Diaz-Peredo E, Sanchez-Solano F, Perez-Reuda E, Bonavides-Martinez C, Collado-Vides J. RegulonDB (version 3.2): transcriptional regulation and operon organization in *Escherichia coli* K-12. *Nucleic Acid Res* 2001;29:72–74.
- Kaasen I, Falkenberg P, Styrvoel OB, Strom Ar. Molecular cloning and physical mapping of the otsBA genes, which encode the osmoregulatory trehalose pathway of *Escherichia coli*: evidence that transcription is activated by katF (AppR). *J Bacteriol* 1992;174:889–898.
- Yan D, Cho H, Hastings CA, Igo MM, Lee S-Y, Pelton JG, Stewart V, Wemmer D, Kustu S. Berylliofluoride mimics phosphorylation of NtrC and other bacterial response regulators. *Proc Natl Acad Sci* 1999;96:14789–14794.
- Double S. Preparation of selenomethionyl proteins for phase determination. *Methods Enzymol* 1997;276:523–529.
- Otwinowski Z, Minor W, editors. Processing of X-ray diffraction data collected in oscillation mode, Vol. 276. New York: Academic Press; 1997. p 307–326.
- Terwilliger TC, Berendzen J. Automated MAD and MIR structure solution. *Acta Crystallographica D* 1999;55:849–861.
- La Fortelle E, Bricogne G. Maximum-likelihood heavy-atom

- parameter refinement: a successful combination of tools for macromolecular structure determination. In: Sweet RM, Carter Jr. CW, editors. *Methods in enzymology, macromolecular crystallography*, Vol. 276. New York: Academic Press; 1997. p 472–494.
25. Terwilliger TC. Maximum likelihood density modification. *Acta Crystallogr D* 2000;56:965–972.
 26. Terwilliger TC. Automated main-chain model-building by template matching and iterative fragment extension. *Acta Crystallogr D* 2002;59:33–44.
 27. Jones TA, Zou JY, Cowan SW, Kjeldgaard M. Improved methods for building protein models in electron density maps and the location of errors in these models. *Acta Crystallogr* 1991;A47:110–119.
 28. Brunger AT, Adams PD. Crystallography and NMR system: a new software suite for macromolecular structure determination. *Acta Crystallogr D* 1998;54:905–921.
 29. Laskowski RA, MacArthur MW. PROCHECK: a program to check the stereochemical quality of protein structures. *J Appl Crystallogr* 1993;26:283–291.
 30. Kraulis EA. MOLSCRIPT: a program to produce both detailed and schematic plots of protein structures. *J Appl Crystallogr* 1991;D50:869–873.
 31. Merritt EA, Bacon DJ. Raster3D photorealistic molecular graphics. *Methods Enzymol* 1997;277:505–524.
 32. DeLano WL. The PyMOL molecular graphics system. <http://www.pymol.org> 2002.
 33. Holm L, Sander C. Protein structure comparison by alignment of distance matrices. *J Mol Biol* 1993;233:123–138.
 34. Lahiri SD, Zhang G, Dunaway-Mariano D, Allen KN. The pentavalent phosphorus intermediate of a phosphoryl transfer reaction. *Science* 2003;299:2067–2071.
 35. Blackburn GM, Williams NH, Gamblin SJ, Smerdon SJ. Comment on “the pentacoordinate phosphorous intermediate of a phosphoryl transfer reaction.” *Science* 2003;301:1184c.
 36. Allen KN, Dunaway-Mariano D. Response to comment on “the pentacoordinate phosphorus intermediate of a phosphoryl transfer reaction.” *Science* 2003;301:1184d.
 37. Altschul SF, Madden TL, Schaffer AA, Zhang AA, Zhang Z, Miller W, Lipman DJ. Gapped BLAST and PSI-BLAST: a new generation of protein database search programs. *Nucleic Acids Res* 1997;25:3389–3402.
 38. Empadinhas N, Marugg JD, Borges N, Santos H, da Costa MS. Pathway for the synthesis of mannosylglycerate in the hyperthermophilic archaeon *Pyrococcus horikoshii*. *J Biol Chem* 2001;276:43580–43588.
 39. Lunn JE, Ashton AR, Hatch MD, Heldt HW. Purification, molecular cloning, and sequence analysis of sucrose-6F-phosphate phosphohydrolase from plants. *Proc Natl Acad Sci* 2000;97:12914–12919.
 40. McCue LA, Thompson W, Carmack CS, Lawrence CE. Factors influencing the identification of transcription factor binding sites by cross-species comparison. *Genome Res* 2002;12:1523–1532.
 41. Lyngstadaas A, Lobner-Olesen A, Grelland E, Boye E. The gene for 2-phosphoglycolate phosphatase (gph) in *Escherichia coli* is located in the same operon as dam and at least five other diverse genes. *Biochim Biophys Acta* 1999;1472:376–384.
 42. Bochner BR, Gadzinski P, Panomitros E. Phenotype microarrays for high-throughput phenotypic testing and assay of gene function. *Genome Res* 2001;11:1246–1255.
 43. Rhodius V, Van Dyk TK, Gross C, LaRossa RA. Impact of genomic technologies on studies of bacterial gene expression. *Annu Rev Microbiol* 2002;56:599–624.
 44. Richmond CS, Glasner JD, Mau R, Jin H, Blattner FR. Genome-wide expression profiling in *Escherichia coli* K-12. *Nucleic Acid Res* 1999;27:3821–3835.
 45. Hughes TR, Marton MJ, Jones AR, Roberts CJ, Stoughton R, Armour CD, Bennett HA, Coffey E, Dai H, He YD, Kidd MJ, King AM, Meyer MR, Slade D, Lum PY, Stepaniants SB, Shoemaker DD, Gachotte D, Chakraburttty K, Simon J, Bard M, Friend SH. Functional discovery via a compendium of expression profiles. *Cell* 2000;102:109–126.
 46. Gonzalez R, Tao H, Shanmugam KT, York SW, Ingram LO. Global gene expression differences associated with changes in glycolytic flux and growth rate in *Escherichia coli* during the fermentation of glucose and xylose. *Biotechnol Prog* 2002;18:6–20.
 47. Allen TE, Herrgard MJ, Liu M, Qiu Y, Glasner JD, Blattner FR, Palsson BO. Genome-scale analysis of the uses of the *Escherichia coli* genome: model-driven analysis of heterogeneous data sets. *J Bacteriol* 2003;185:6392–6399.
 48. Glasner JD, Liss P, Plunkett G, Darling A, Prasad T, Rusch M, Byrnes A, Gilson M, Biehl B, Blattner FR. ASAP, a systematic annotation package for community analysis of genomes. *Nucleic Acid Res* 2003;31:147–151.
 49. Robison K, McGuire AM, Church GM. A comprehensive library of DNA-binding site matrices for 55 proteins applied to the complete *Escherichia coli* K12 genome. *J Mol Biol* 1998;284:241–254.
 50. Beitz E. TeXshade: Shading and labelling of multiple sequence alignments using latex2ε. *Bioinformatics* 2000;16:135–139.